Journal of *Marine Science and Engineering*

MDPI

Article

A Comparative Study on Energy Consumption Forecast Methods for Electric Propulsion Ship

Ji-Yoon Kim [1], Jong-Hak Lee [2], Ji-Hyun Oh [2] and Jin-Seok Oh [3,*]

[1] Romantique, Contents AI Research Center, 27 Daeyeong-ro, Busan 49227, Korea; rlawldbs2918@nate.com
[2] Graduate School, Korea Maritime and Ocean University, 727 Taejong-ro, Yeongdo-gu, Busan 49112, Korea; dldllld@g.kmou.ac.kr (J.-H.L.); ozii@g.kmou.ac.kr (J.-H.O.)
[3] Division of Marine System Engineering, Korea Maritime and Ocean University, 727 Taejong-ro, Yeongdo-gu, Busan 49112, Korea
* Correspondence: ojs@kmou.ac; Tel.: +82-51-410

Abstract: Efficient vessel operation may reduce operational costs and increase profitability. This is in line with the direction pursued by many marine industry stakeholders such as vessel operators, regulatory authorities, and policymakers. It is also financially justifiable, as fuel oil consumption (FOC) maintenance costs are reduced by forecasting the energy consumption of electric propulsion vessels. Although recent technological advances demand technology for electric propulsion vessel electric power load forecasting, related studies are scarce. Moreover, previous studies that forecasted the loads excluded various factors related to electric propulsion vessels and failed to reflect the high variability of loads. Therefore, this study aims to examine the efficiency of various multialgorithms regarding methods of forecasting electric propulsion vessel energy consumption from various data sampling frequencies. For this purpose, there are numerous machine learning algorithm sets based on convolutional neural network (CNN) and long short-term memory (LSTM) combination methods. The methodology developed in this study is expected to be utilized in training the optimal energy consumption forecasting model, which will support tracking of degraded performance in vessels, optimize transportation, reflect emissions accurately, and be applied ultimately as a basis for route optimization purposes.

Keywords: smart ship; energy management; prediction of power; long short-term memory models; bidirectional long short-term memory models

Citation: Kim, J.-Y.; Lee, J.-H.; Oh, J.-H.; Oh, J.-S. A Comparative Study on Energy Consumption Forecast Methods for Electric Propulsion Ship. *J. Mar. Sci. Eng.* **2022**, *10*, 32. https://doi.org/10.3390/jmse10010032

Received: 21 November 2021
Accepted: 27 December 2021
Published: 30 December 2021

1. Introduction

The International Maritime Organization (IMO) 2020 rule strengthened the regulations for preventing marine environmental pollution. Emission gas standard restrictions have become more stringent, such as mandating 0.1% low sulfur oil fuel use in emission control areas (ECAs) [1–3]. Thus, environmentally friendly vessels (typically electric propulsion vessels) have been actively studied for replacing conventional vessels [4–6].

When designing an electric propulsion system, it is necessary to estimate the ship's power consumption, which is essential to determine the ship's FOC, in order to plan the ship's route [7–10]. In general, the method proposed by the International Organization for Standardization (ISO) is widely used to predict the power of a ship. However, it is known that this method is not suitable for practical use when the weather conditions are good. Therefore, there is a need for a method that can more accurately predict the power of a ship [11–15].

Traditionally, numerical methods using model test results have been widely used to predict ship power. However, it is difficult to predict the power of a vessel due to the uncertainty of model testing [16–20].

In order to solve the uncertainty of the predictive model, on-board testing should be performed. However, it requires considerable resources and time [21–25]. Therefore,

it is difficult to predict the operational capability of a ship using numerical methods. In several studies, ship power was predicted using data-driven models [26–28]. There are two representative data-driven methods used to predict the power of a vessel: regression analysis and deep learning methods. Regression analysis is a method of identifying correlations between multiple variables. This method can quickly generate predictive models for simple problems.

Deep learning, a type of machine learning based on artificial neural networks, is an effective way to predict data patterns. With sufficient training data, deep learning can solve complex problems more effectively than regression analysis. In addition, depending on the complexity of the problem, deep learning models can be tuned. Therefore, the purpose of this study is to investigate the efficiency of various multialgorithms based on deep learning to predict electric propulsion energy consumption.

For this purpose, there are various deep learning algorithm sets depending on convolutional neural network (CNN) and long short-term memory (LSTM) combination methods. The remaining sections of this article are structured as follows: Section 2 illustrates the research background as well as an outline of previous attempts on power forecasting. Section 3 provides a detailed description of the data for the experiment and the proposed methodology. In Section 4, the process and results for validating the proposed model are presented and discussed. Finally, Section 5 provides a conclusion.

2. Methodology

2.1. Dataset Acquisition

The propulsion power consumes approximately 90% of the total power in an electric propulsion vessel. Therefore, forecasting the propulsion power load is necessary to estimate the total energy consumption [29,30]. The propulsion power load is related to the vessel speed and hull resistance [31,32]. Frictional resistance and residual resistance components of a ship's total resistance play an important role because they account for the largest portion of the total ship resistance of most merchant ships. The total resistance of the vessel can be calculated by the following Equation (1) [33]:

$$R_T = R_F + R_R \tag{1}$$

where R_T, R_F, and R_R are the total resistance, friction resistance, and residual resistance, respectively. The resistor components above are calculated using the general form (2):

$$R = \frac{1}{2}\rho C A V^2 \tag{2}$$

where C is the resistance coefficient, ρ [kg/m^3] is the density of the medium, A [m^2] is the wetted surface area, and V [m/s] is the speed of the vessel.

Since the effective horsepower changes according to the above resistance, its value can be known through Equation (3), below:

$$P_E = R_T \times V \tag{3}$$

where P_E is effective power. Therefore, this study selected data related to the propulsion power of electric vessels using Equations (1)–(3). The water depth, current speed, wind direction, wind speed, and draft data directly determine vessel resistance and, indirectly, the vessel direction, direction key angle, vessel speed, and main engine rotational speed [34]. The selected data types used in this study are compiled in Table 1.

Table 1. List of selected data.

Item	Unit	Remark
Electric Load	kW	800–40,000
Propulsion Load	HP	0–65,536
Heading Angle	Degree	0–360°
Rudder Angle	Degree	−35–35°
Water Depth	M	0–836
Water Speed	m/s	−4–6
Wind Angle	Degree	0–360°
Wind Speed	m/s	0–47
Vessel Speed	knot	0–25
M/E RPM	Rpm	0–76.3
Draft (after)	m	0–15.4
Draft (forward)	m	0–18.8
Draft (Port)	m	0–15.6
Draft (Starboard)	m	0–16.38

Because the electric load used varies depending on the mode of ship's operation, it is classified as shown in Table 2. Table 2 lists all of the ship's loads, including propulsion system loads, power generation system loads, cooling system loads, oil system loads, and boiler system loads. Figure 1 depicts the target ship's route.

Table 2. List of electrical loads.

Classification	SEA Going	Port in/out	Cargo Unload
Continuous Load (kW)	2299.9	2660.4	1916
Reffer Container Load (kW)	7440	7440	7440
Intermittent Load (kW)	337.5	375.2	440.9
Group Diversity Factor (-)	0.4	0.4	0.4
Actual Intermittent Load (kW)	135	150.1	176.4
Deck Machinery Load (kW)	0	3,637.2	286

Figure 1. Navigation route.

2.2. Modeling Methodologies

2.2.1. CNN–LSTM (Direct)

The time-series data are entered into a one-dimensional (1D) CNN, and the time-series data features extracted from the 1D CNN are entered into a three-class LSTM [35–37]. Then, the following forecast value is printed out using the weight and activation function that were learned in the LSTM [38]. Figure 2 presents the CNN–LSTM (direct)-based model structure.

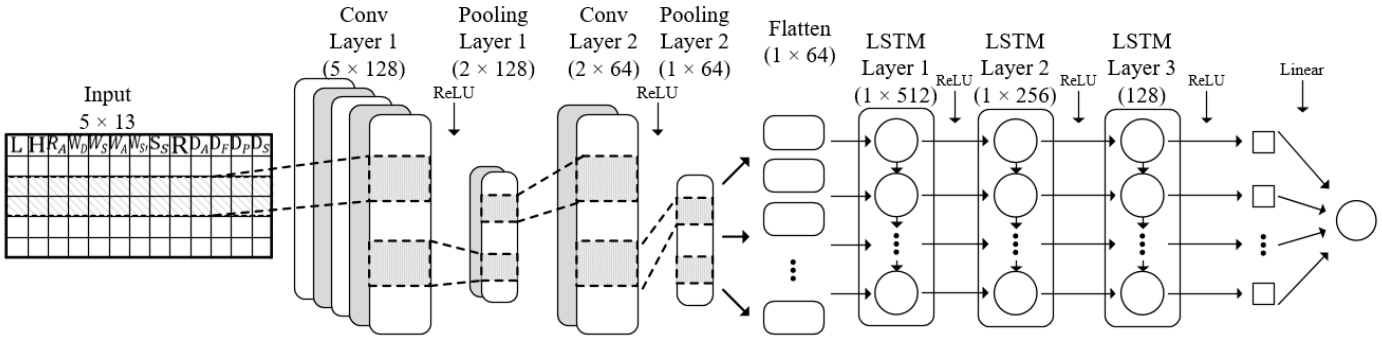

Figure 2. Construction of CNN–LSTM (direct).

2.2.2. CNN–LSTM (Parallel)

The time-series data are entered into a one-dimensional (1D) CNN, and the time-series data features extracted from the 1D CNN are entered into a three-class LSTM. Then, the following forecast value is printed out using the weight and activation function that were learned in the LSTM. Figure 3 presents the CNN–LSTM (parallel)-based model structure.

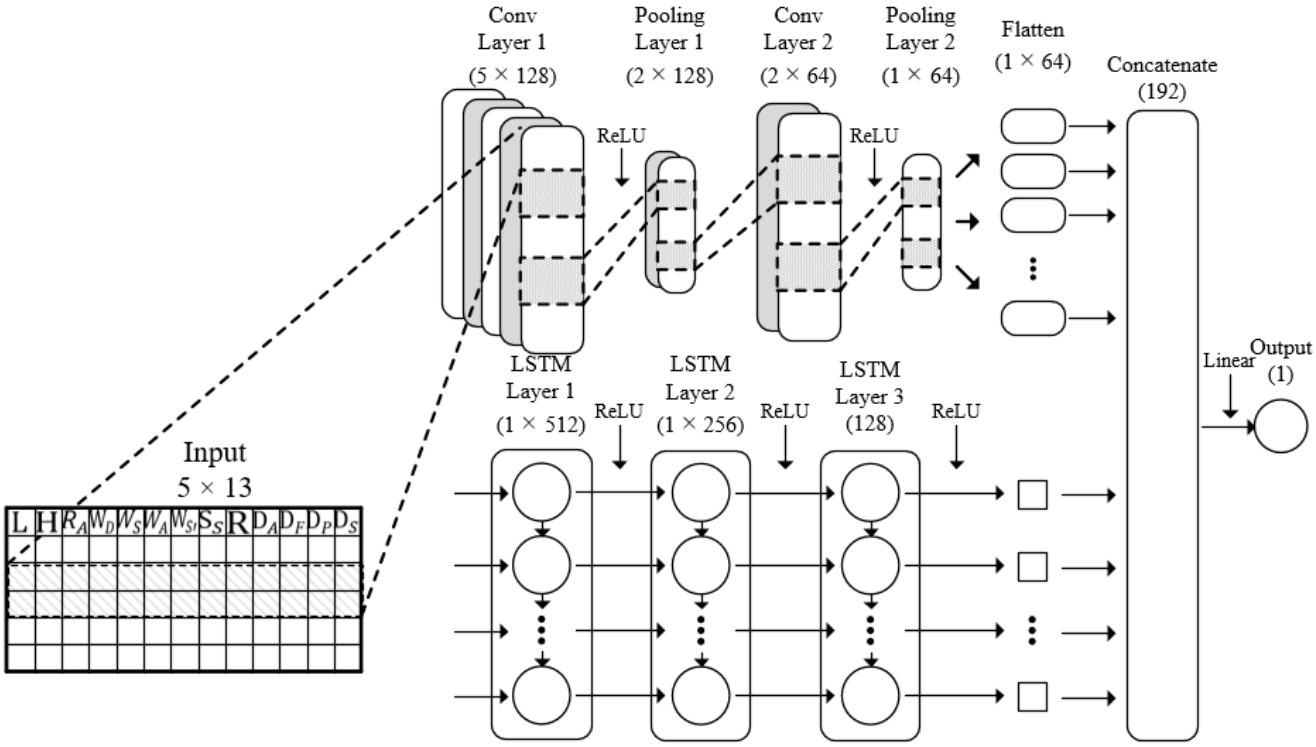

Figure 3. Construction of CNN–LSTM (parallel).

2.2.3. CNN–Bidirectional LSTM (Direct)

The time-series data are entered into a 1D CNN, and the corresponding features extracted are entered into a three-class bidirectional LSTM [39]. In sequence, the following

forecast value is printed out using the weight and activation function learned in the bidirectional LSTM. Figure 4 presents the CNN–bidirectional LSTM (direct)-based model structure.

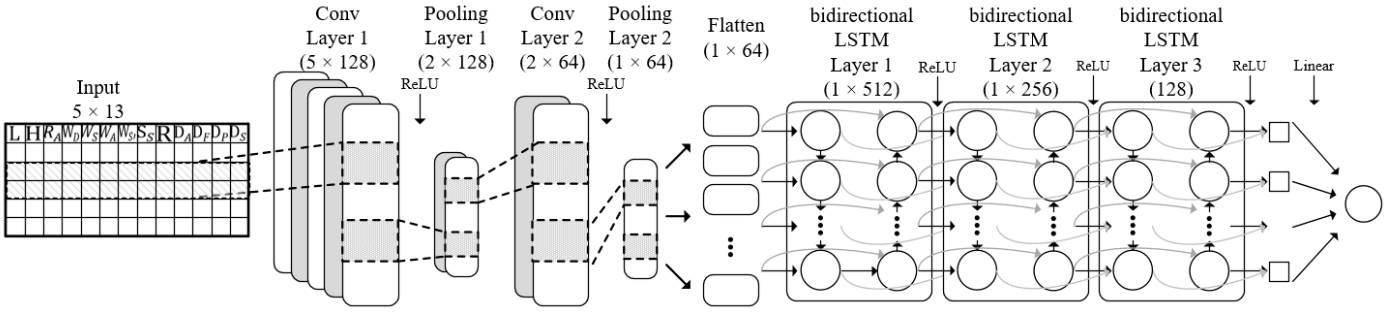

Figure 4. Construction of CNN–bidirectional LSTM (direct).

2.2.4. CNN–Bidirectional LSTM (Parallel)

The analysis results of the data features learned in the CNN and the time-series forecasting data learned in the bidirectional LSTM are combined to enable time-series forecasting. The following forecast value is printed out using the weight and activation function learned in the CNN and bidirectional LSTM. Figure 5 presents the CNN–bidirectional LSTM (parallel)-based model structure.

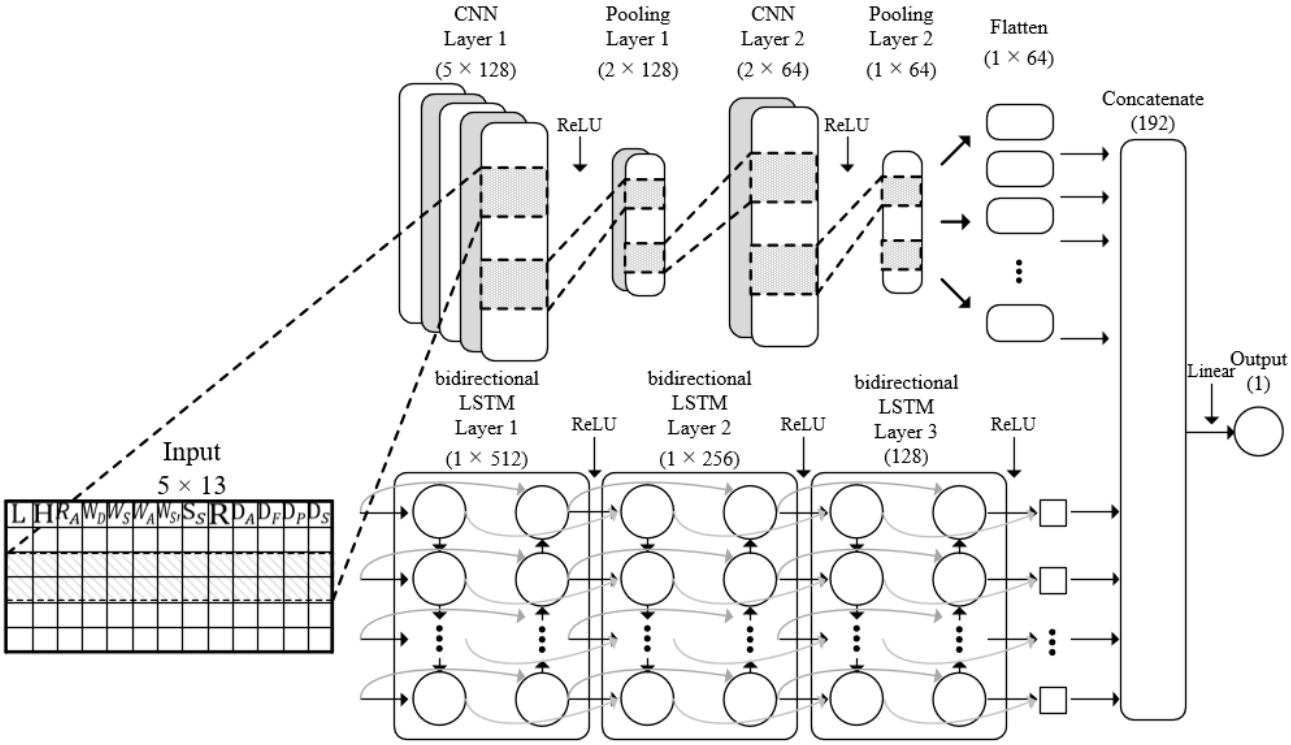

Figure 5. Construction of CNN–bidirectional LSTM (parallel).

This structure can be described as follows: (1) extracting the features of the electric propulsion vessel data that were entered into the CNN and (2) synthesizing data existing in the previous time slot with the time-series data forecast value from the classified results, the hidden layer performance improvement learned from the bidirectional LSTM, and a time-series data forecasting (with no loss of previous time information regardless of the data length and layer) to show its output.

2.3. Experiment Procedures

The data recorded every 10 min from an operating container vessel was used as the dataset, which was stored for approximately 205 days. Then, the data that affected the vessel power load were selected and merged into 14 variables. In addition, data standardization was applied to learning, training, and validation. Here, the training data refers to the data to be used in model training, and test data is used in assessing training accuracy. The validation data are used to solve overfitting and to improve the performance of a model that utilizes training data for learning. Finally, this study selected the ratios for learning, training, and validation data, which were obtained as a result of base model testing to solve forecasting model overfitting. The learning-to-training data and training-to-validation dataset ratios used were 7:3. Figure 6 shows the training and learning data ratios.

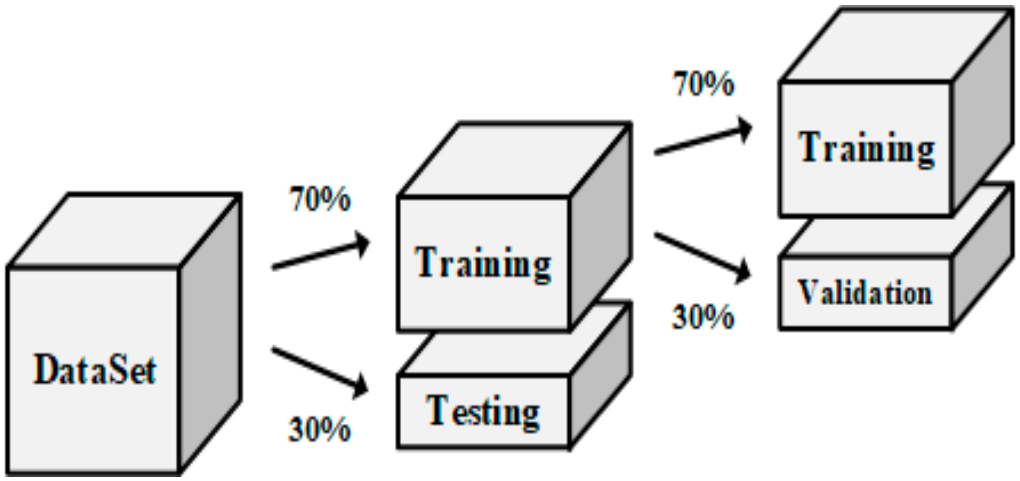

Figure 6. Separate data with training and testing datasets.

Minibatch gradient descent was used to accelerate the training [40,41]. The batch size was 512, the learning rate was 0.001, and the number of epochs was 500. Early stopping was set to prevent overfitting during learning. Moreover, the patience of early stopping was set to 100 to configure the model to learn the optimal value. Figure 7 shows the learning procedure.

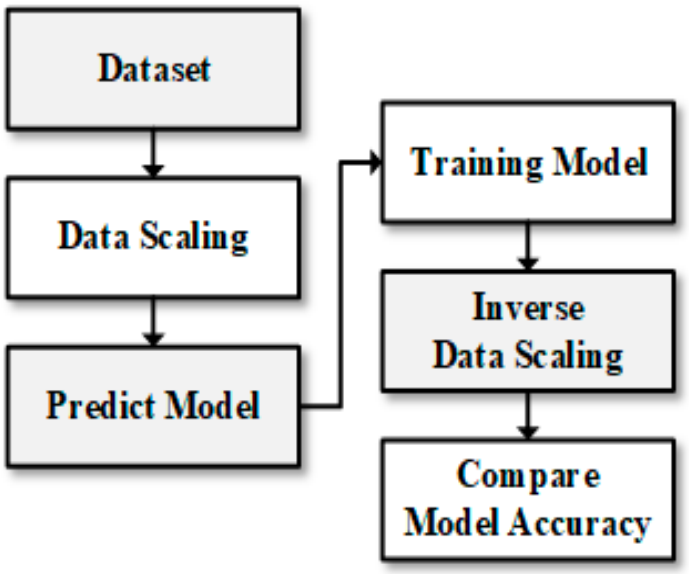

Figure 7. Learning procedure.

The dataset was scaled for accurate data learning. The scaled data were entered into each model presented in Section 2.2 to proceed with learning. The values forecasted by models that completed learning were compared with actual values after inverse scaling [42]. The root-mean-square error (RMSE) value was used to assess the comparison with the actual value, and the best-performing model was selected after comparing the actual value of each model with the forecast value [43]. Time step, which is a numerical value that represents the number of trials constituting the data forecast for configuring the forecasting program, was selected to generate time-series data. The time step value size can be adjusted depending on the variation in the previous time value that is intended for use. Generally, a larger time step value leads to a vanishing gradient problem [44–46]. This study presented data measured every 10 min; thus, setting the time step value to 1 indicates using one set of data of 10 min ago to forecast the power load after 10 min. This study configured the power load in the upcoming 10 min to be forecasted according to the data variation in the previous 50 min. Therefore, the time step was set to five.

2.4. Design Implementation of Models

Forecasting models in various structures were used in this study to identify their power load forecast accuracies. The previous AI model for power load forecasting was used for forecasting a relatively narrow range (0–100 kW) of power values, and the power load variability was low. However, the forecasting power load range is relatively wide (0–40,000 kW) for electric propulsion vessels. Therefore, a model that could best forecast within the power load range of electric propulsion vessels and its variability was required in this study. For this purpose, various models were tested to select the one with the highest load forecasting performance. Table 3 summarizes the application of the designed models.

Table 3. Summary of model structures.

Model Structure	Combination Method	Detail
CNN–LSTM	Direct	CNN: (5 × 128) − (2 × 128) − (2 × 64) − (64) LSTM: (1 × 512) − (1 × 256) − (128)
CNN–bidirectional LSTM	Direct	CNN: (5 × 128) − (2 × 128) − (2 × 64) − (64) bidirectional LSTM: (1 × 512) − (1 × 256) − (128)
CNN–LSTM	Parallel	CNN: (5 × 128) − (2 × 128) − (2 × 64) − (64) LSTM: (1 × 512) − (1 × 256) − (128)
CNN–bidirectional LSTM	Parallel	CNN: (5 × 128) − (2 × 128) − (2 × 64) − (64) bidirectional LSTM: (1 × 512) − (1 × 256) − (128)

3. Validation of Generalization Capabilities of the Models

This section may be divided by subheadings. It should provide a concise and precise description of the experimental results, their interpretation, and the experimental conclusions that can be drawn.

This study employed the RMSE method to assess model performances [47,48]. In addition, the following assessment criteria were established:

1. All data used in learning and assessing were equal, and learning was repeated five times.
2. All LSTM and CNN hyperparameters were tuned equally for every model combination, and RMSE was used. The stored RMSE data distribution was used when comparing model performances.
3. Statistical analysis was performed using the RMSE value obtained from repeated learning when comparing model performances.
    - Average value: used as a value representing performance;
    - Standard deviation: used as an indicator for assessing dispersion;

- Minimum value: used for estimating standard deviation;
- Quartile: use range of learning results set;
- Maximum value: used for estimating standard deviation.

4. Evaluation functions such as precision or recall, which are used for classification, were not considered numeric data and used for learning. The proximity between the forecast and actual values was considered instead.

Figure 8 presents the forecast results from all models with the entire data. Five learning cycles were conducted, and the learning result of the degrees that showed the lowest RMSE from each model was used and expressed to evaluate the forecast results. Figure 8 presents the results expressed in terms of representative times to identify detailed forecast results.

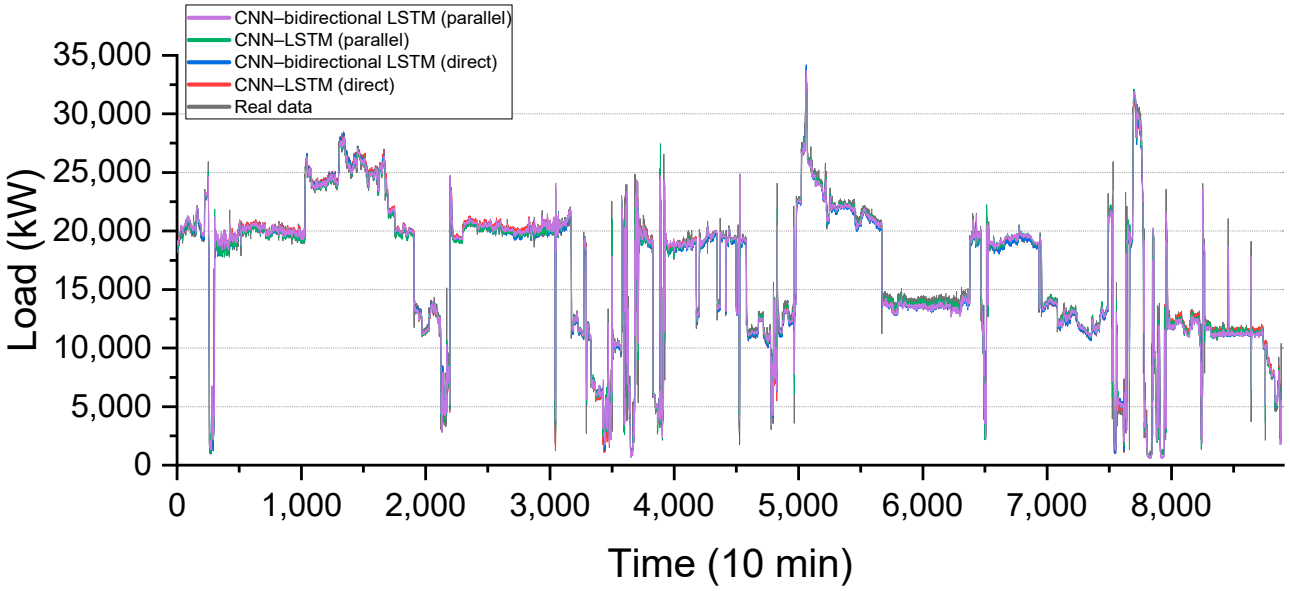

Figure 8. Result of forecasts by each model.

By comparing the forecast results with the actual data in Figures 8 and 9, a tendency according to data variations was identifiable from the LSTM model forecast results, but an overall higher value was forecasted compared to the actual value. Additionally, high accuracy was observed in forecasts for heavy loading use or operational mode change. A tendency according to data variations was identifiable from the bidirectional LSTM model forecasts results, but an overall lower value was forecasted compared to the actual value. Additionally, forecasts between 10–15 MWh were unstable. The results of the CNN–LSTM (direct) and CNN–bidirectional LSTM (direct) models forecasted the tendency according to data variations and similar forecasted and actual values. However, their forecasts on the short-term tendency were low. Moreover, the tendency according to rapid load variations due to heavy loading could be forecasted, but the variation range was narrow to prepare for variations in the actual value. The data tendency forecast performance was high from the forecast results of the CNN–LSTM (parallel) and CNN–bidirectional LSTM (parallel), and the difference between the actual and forecast values was low. Furthermore, high performance was observed for the tendency according to rapid load variations due to heavy loading and wide variation range. However, values obtained for the CNN–bidirectional LSTM (parallel) model were lower than actual values for the 10–15 MWh forecasts.

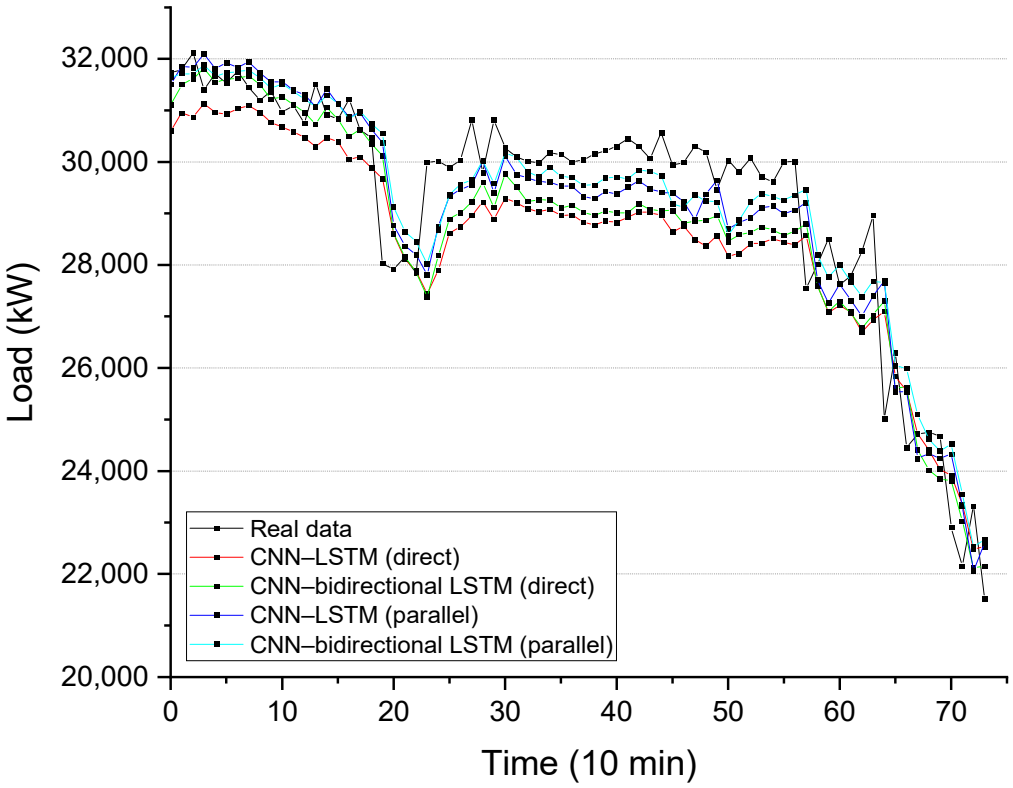

Figure 9. Result of forecast by each model in detail.

4. Results and Discussion

The RMSE scores were calculated for the learning results and are summarized in Table 4. The RMSE statistics based on the five initial learning results are presented in Table 5.

Table 4. RMSE results of each model experiment.

Model	Combination Method	1st	2nd	3rd	4th	5th
CNN–LSTM	Direct	1752.0	1679.3	1869.2	1806.6	1523.6
CNN–bidirectional LSTM	Direct	1670.7	1534.4	1501.7	1536.3	1520.2
CNN–LSTM	Parallel	1461.0	1552.0	1476.6	1512.9	1507.6
CNN–bidirectional LSTM	Parallel	1579.1	1514.4	1501.9	1509.1	1484.0

The CNN–LSTM (parallel) model displayed the highest performance at 1502. In particular, the CNN–LSTM combination in parallel composition was identified to better forecast the power load compared to the CNN–LSTM (direct). The error rate comparison between models in Table 4 is presented in Figure 10.

Table 5. Statistical information of RMSE of experiment results.

Model	Combination Method	Average	Standard Deviation	Min Value	4-Quantiles			Max Value
					25%	50%	75%	
CNN–LSTM	Direct	1726.1	133.0	1523.6	1679	1752	1806	1869.2
CNN–bidirectional LSTM	Direct	1552.7	67.4	1501.7	1520	1534	1536	1670.7
CNN–LSTM	Parallel	1502.0	35.3	1461	1476	1507	1512	1552
CNN–bidirectional LSTM	Parallel	1517.7	36.2	1484	1501	1509	1514	1579.1

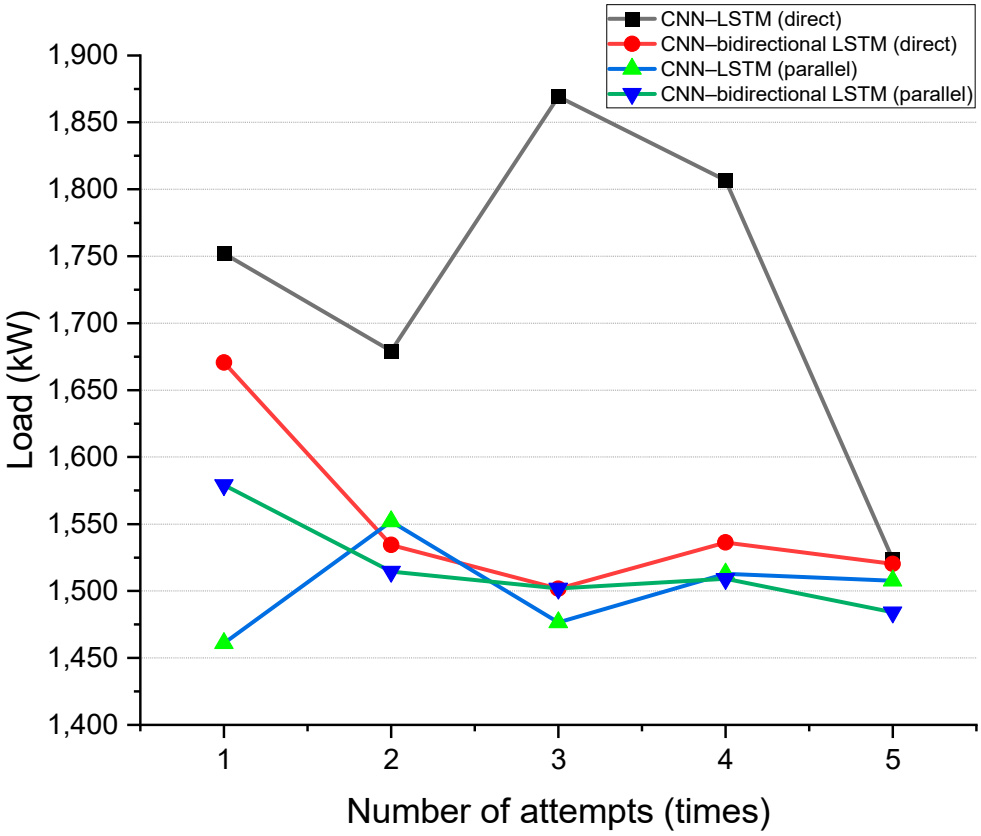

Figure 10. Comparison of RMSE values for different models.

The following results were obtained by analyzing Figure 9. The RMSE scores largely varied for each learning in the CNN–LSTM (direct) model. Large RMSE were generated in the first and third tests in the CNN–bidirectional LSTM (direct) model. The model error was the lowest for each learning in the CNN–LSTM (parallel) model. The error rate in the CNN–bidirectional LSTM (parallel) model was lower than that of the CNN–bidirectional LSTM (direct) model. However, when considering the RMSE comparison, the CNN–bidirectional LSTM (parallel) model had relatively lower performance than the CNN–LSTM (parallel) model. The analysis results showed that the LSTM or bidirectional LSTM and the CNN combination models had higher power data forecasting performance than other models. The following conclusions were obtained after analysis for identifying the model with the highest performance: (1) the CNN–bidirectional LSTM (direct, parallel) models exhibited good performances but generated outliers, and (2) the CNN–LSTM (parallel) model had

lower error rate distribution compared to the CNN–bidirectional LSTM (parallel) model but had no outliers and good performance.

5. Conclusions

The forecasting model for the electric propulsion vessel with high load variability was analyzed using the previous study results and AI model analysis. In this study, data feature extraction and time-series data forecasting were emphasized. The initial speculation of the electric propulsion power load forecast model of the vessel, which utilized a combined CNN model and the time-series data model, predicted that the CNN–LSTM (direct) model would show high performance. In the CNN–LSTM (direct) model, the CNN model extracts the data features, and the time-series forecasting is performed in the time-series data model such as the LSTM using the extracted data. However, experimental results showed that the CNN–LSTM (parallel) model performance was high. Additionally, it was identified that when the time-series data forecasting and data feature extraction proceeded separately, the model that synthesized the result values forecasted with high performance.

Various forecasting models were tested to compare their performances. First, a CNN that can extract data features using various variables was used, and the CNN–LSTM and CNN–bidirectional LSTM models were distinguished by their combination methods. The model experiments were repeated five times for each model, and the RMSE scores were used to analyze the performances of models by comparing their average RMSE and boxplot normal distribution. The RMSE value for the LSTM, bidirectional LSTM, CNN–LSTM (direct), CNN–bidirectional LSTM (direct), CNN–LSTM (parallel), and CNN–bidirectional LSTM (parallel) models were 1747.7, 1704, 1726.1, 1522.7, 1502, and 1517.7, respectively, and the best performance was observed for the CNN–LSTM (parallel) model. The boxplot analysis results showed that the CNN–LSTM (parallel) structure was the most stable model, as it did not show outliers. As a black box approach, this model does not require additional domain knowledge to be derived. Therefore, this methodology can be essentially applied to all vessels to track degraded performances, optimize transportation, and reflect vessel emissions accurately and ultimately be used to create a model that supports its use as a basis for route optimization purposes.

Author Contributions: Conceptualization, Methodology, J.-Y.K.; Software, Validation, Data curation, J.-Y.K., J.-H.L. and J.-H.O.; Writing—original draft preparation, review and editing, J.-H.L. and J.-H.O., Project administration, Funding acquisition, J.-S.O. All authors have read and agreed to the published version of the manuscript.

Funding: This work was supported by the Ministry of Education of the Republic of Korea and the National Research Foundation of Korea (NRF-2018R1D1A1B07049361).

Institutional Review Board Statement: Not applicable.

Informed Consent Statement: Not applicable.

Data Availability Statement: Not applicable.

Conflicts of Interest: The authors declare no conflict of interest.

References

1. Bodansky, D. Regulating greenhouse gas emissions from ships: The role of the International Maritime Organization. In *Ocean Law Debates*; Brill Nijhoff: Santa Cruz, CA, USA, 2018; pp. 478–501.
2. Joung, T.-H.; Kang, S.-G.; Lee, J.-K.; Ahn, J. The IMO initial strategy for reducing Greenhouse Gas (GHG) emissions, and its follow-up actions towards 2050. *J. Int. Marit. Saf. Environ. Aff. Shipp.* **2020**, *4*, 1–7. [CrossRef]
3. Serra, P.; Fancello, G. Towards the IMO's GHG goals: A critical overview of the perspectives and challenges of the main options for decarbonizing international shipping. *Sustainability* **2020**, *12*, 3220. [CrossRef]
4. Kose, S.; Sekban, D.; Ozkok, M. Determination of port-induced exhaust gas emission amounts and investigation of environmental impact by creating emission maps: Sample of Trabzon port. *Int. J. Sustain. Transp.* **2021**, *15*, 1–11. [CrossRef]
5. Reusser, C.A.; Pérez Osses, J.R. Challenges for Zero-Emissions Ship. *J. Mar. Sci. Eng.* **2021**, *9*, 1042. [CrossRef]
6. Saxe, H.; Larsen, T. Air pollution from ships in three Danish ports. *Atmos. Environ.* **2004**, *38*, 4057–4067. [CrossRef]

7. Cardoso, A.J.M.; Popkov, E.; Koptjaev, E. Evolution and development prospects of electric propulsion systems of large sea ships. In Proceedings of the 2020 International Ural Conference on Electrical Power Engineering (UralCon), Chelyabinsk, Russia, 22–24 September 2020; pp. 296–303.
8. Hansen, J.F.; Wendt, F. History and state of the art in commercial electric ship propulsion, integrated power systems, and future trends. *Proc. IEEE* **2015**, *103*, 2229–2242. [CrossRef]
9. McCoy, T.J. Trends in ship electric propulsion. In Proceedings of the IEEE Power Engineering Society Summer Meeting, Chicago, IL, USA, 21–25 July 2002; pp. 343–346.
10. Pestanam, H. Future trends of electric propulsion and implications to ship design. *Proc. Martech* **2014**, *1*, 1–10.
11. Sáiz, V.M.M.; López, A.P. Future trends in electric propulsion systems for commercial vessels. *J. Marit. Res.* **2007**, *4*, 81–100.
12. Kanellos, F.D.; Anvari-Moghaddam, A.; Guerrero, J.M. A cost-effective and emission-aware power management system for ships with integrated full electric propulsion. *Electr. Power Syst. Res.* **2017**, *150*, 63–75. [CrossRef]
13. Nuchturee, C.; Li, T.; Xia, H. Energy efficiency of integrated electric propulsion for ships—A review. *Renew. Sustain. Energy Rev.* **2020**, *134*, 110–145. [CrossRef]
14. Xie, C.; Zhang, C. Research on the ship electric propulsion system network power quality with flywheel energy storage. In Proceedings of the 2010 Asia-Pacific Power and Energy Engineering Conference, Chengdu, China, 28–31 March 2010; pp. 1–3.
15. Kim, Y.-R.; Kim, J.-M.; Jung, J.-J.; Kim, S.-Y.; Choi, J.-H.; Lee, H.-G. Comprehensive Design of DC Shipboard Power Systems for Pure Electric Propulsion Ship Based on Battery Energy Storage System. *Energies* **2021**, *14*, 5264. [CrossRef]
16. Kim, K.; Park, K.; Ahn, J.; Roh, G.; Chun, K. A study on applicability of Battery Energy Storage System (BESS) for electric propulsion ships. In Proceedings of the 2016 IEEE Transportation Electrification Conference and Expo, Asia-Pacific (ITEC Asia-Pacific), Busan, Korea, 1–4 June 2016; pp. 203–207.
17. He, Y.; Fan, A.; Wang, Z.; Liu, Y.; Mao, W. Two-phase energy efficiency optimisation for ships using parallel hybrid electric propulsion system. *Ocean Eng.* **2021**, *238*, 1–12. [CrossRef]
18. Zhu, J.; Chen, L.; Wang, X.; Yu, L. Bi-level optimal sizing and energy management of hybrid electric propulsion systems. *Appl. Energy* **2020**, *260*, 114–134. [CrossRef]
19. Jaster, T.; Rowe, A.; Dong, Z. Modeling and simulation of a hybrid electric propulsion system of a green ship. In Proceedings of the 2014 IEEE/ASME 10th International Conference on Mechatronic and Embedded Systems and Applications (MESA), Senigallia, Italy, 10–12 September 2014; pp. 1–6.
20. Geertsma, R.; Negenborn, R.; Visser, K.; Hopman, J. Design and control of hybrid power and propulsion systems for smart ships: A review of developments. *Appl. Energy* **2017**, *194*, 30–54. [CrossRef]
21. Kim, K.; An, J.; Park, K.; Roh, G.; Chun, K. Analysis of a supercapacitor/battery hybrid power system for a bulk carrier. *Appl. Sci.* **2019**, *9*, 1547. [CrossRef]
22. Yuan, Y.; Zhang, T.; Shen, B.; Yan, X.; Long, T. A fuzzy logic energy management strategy for a photovoltaic/diesel/battery hybrid ship based on experimental database. *Energies* **2018**, *11*, 2211. [CrossRef]
23. Ovrum, E.; Bergh, T. Modelling lithium-ion battery hybrid ship crane operation. *Appl. Energy* **2015**, *152*, 162–172. [CrossRef]
24. Lan, H.; Wen, S.; Hong, Y.-Y.; David, C.Y.; Zhang, L. Optimal sizing of hybrid PV/diesel/battery in ship power system. *Appl. Energy* **2015**, *158*, 26–34. [CrossRef]
25. Hou, J.; Sun, J.; Hofmann, H. Adaptive model predictive control with propulsion load estimation and prediction for all-electric ship energy management. *Energy* **2018**, *150*, 877–889. [CrossRef]
26. Lim, C.-O.; Park, B.-C.; Lee, J.-C.; Kim, E.S.; Shin, S.-C. Electric power consumption predictive modeling of an electric propulsion ship considering the marine environment. *Int. J. Nav. Archit. Ocean Eng.* **2019**, *11*, 765–781. [CrossRef]
27. Gao, D.; Jiang, Y.; Zhao, N. A novel load prediction method for hybrid electric ship based on working condition classification. *Trans. Inst. Meas. Control.* **2020**, *44*, 5–14. [CrossRef]
28. Xiao, J.; Zhang, T.; Wang, X. Ship power load prediction based on RST and RBF neural networks. In Proceedings of the International Symposium on Neural Networks, Chongqing, China, 30 May–1 June 2005; pp. 648–653.
29. Zhang, Q.; Zhang, H.; Chen, Y. Electric Power Load Prediction based on Temporal Semantic Information and LSTM. In Proceedings of the 2020 Eighth International Conference on Advanced Cloud and Big Data (CBD), Taiyuan, China, 5–6 December 2020; pp. 153–156.
30. Ma, Y.; Oslebo, D.; Maqsood, A.; Corzine, K. Pulsed-Power Load Monitoring for an All-Electric Ship: Utilizing the Fourier Transform Data-Driven Deep Learning Approach. *IEEE Electrif. Mag.* **2021**, *9*, 25–35. [CrossRef]
31. Hou, J.; Sun, J.; Hofmann, H. Control development and performance evaluation for battery/flywheel hybrid energy storage solutions to mitigate load fluctuations in all-electric ship propulsion systems. *Appl. Energy* **2018**, *212*, 919–930. [CrossRef]
32. Xiros, N.I.; Kyrtatos, N.P. A neural predictor of propeller load demand for improved control of diesel ship propulsion. In Proceedings of the 2000 IEEE International Symposium on Intelligent Control. Held Jointly with the 8th IEEE Mediterranean Conference on Control and Automation (Cat. No. 00CH37147), Patras, Greece, 19 July 2000; pp. 321–326.
33. Elkafas, A.G.; Elgohary, M.M.; Zeid, A.E. Numerical study on the hydrodynamic drag force of a container ship model. *Alex. Eng. J.* **2019**, *58*, 849–859. [CrossRef]
34. Molland, A.F.; Turnock, S.R.; Hudson, D.A. *Ship Resistance and Propulsion*; Cambridge University Press: Cambridge, UK, 2017.
35. Valueva, M.V.; Nagornov, N.; Lyakhov, P.A.; Valuev, G.V.; Chervyakov, N.I. Application of the residue number system to reduce hardware costs of the convolutional neural network implementation. *Math. Comput. Simul.* **2020**, *177*, 232–243. [CrossRef]

36. Chen, Y.; Kang, Y.; Chen, Y.; Wang, Z. Probabilistic forecasting with temporal convolutional neural network. *Neurocomputing* **2020**, *399*, 491–501. [CrossRef]
37. Mittelman, R. Time-series modeling with undecimated fully convolutional neural networks. *arXiv* **2015**, arXiv:1508.00317.
38. Gers, F.A.; Schmidhuber, J.; Cummins, F. Learning to forget: Continual prediction with LSTM. *Neural Comput.* **2000**, *12*, 2451–2471. [CrossRef] [PubMed]
39. Schuster, M.; Paliwal, K.K. Bidirectional recurrent neural networks. *IEEE Trans. Signal Process.* **1997**, *45*, 2673–2681. [CrossRef]
40. Khirirat, S.; Feyzmahdavian, H.R.; Johansson, M. Mini-batch gradient descent: Faster convergence under data sparsity. In Proceedings of the 2017 IEEE 56th Annual Conference on Decision and Control (CDC), Melbourne, Australia, 12–15 December 2017; pp. 2880–2887.
41. Hinton, G.; Srivastava, N.; Swersky, K. Neural networks for machine learning lecture 6a overview of mini-batch gradient descent. *Cited* **2012**, *14*, 2.
42. Al-Mohy, A.H.; Higham, N.J. Improved inverse scaling and squaring algorithms for the matrix logarithm. *SIAM J. Sci. Comput.* **2012**, *34*, 153–169. [CrossRef]
43. Agresti, A. *Categorical Data Analysis*; John Wiley & Sons: Hoboken, NJ, USA, 2003; Volume 482.
44. Hochreiter, S. The vanishing gradient problem during learning recurrent neural nets and problem solutions. *Int. J. Uncertain. Fuzziness Knowl.-Based Syst.* **1998**, *6*, 107–116. [CrossRef]
45. Hochreiter, S. Recurrent neural net learning and vanishing gradient. *Int. J. Uncertain. Fuzziness Knowl.-Based Syst.* **1998**, *6*, 107–116.
46. Hu, Y.; Huber, A.; Anumula, J.; Liu, S.-C. Overcoming the vanishing gradient problem in plain recurrent networks. *arXiv* **2018**, arXiv:1801.06105.
47. Chai, T.; Draxler, R.R. Root mean square error (RMSE) or mean absolute error (MAE). *Geosci. Model Dev. Discuss.* **2014**, *7*, 1525–1534.
48. Willmott, C.J.; Matsuura, K. Advantages of the mean absolute error (MAE) over the root mean square error (RMSE) in assessing average model performance. *Clim. Res.* **2005**, *30*, 79–82. [CrossRef]